Dynamic JUNQ inclusion bodies are asymmetrically inherited in mammalian cell lines through the asymmetric partitioning of vimentin

Mikołaj Ogrodnik[1], Hanna Salmonowicz[1], Rachel Brown, Joanna Turkowska, Władysław Średniawa, Sundararaghavan Pattabiraman, Triana Amen, Ayelet-chen Abraham, Noam Eichler, Roman Lyakhovetsky, and Daniel Kaganovich[2]

Department of Cell and Developmental Biology, Alexander Silberman Institute of Life Sciences, Hebrew University of Jerusalem, Jerusalem 91904, Israel

Edited by Gregory A. Petsko, Weill Cornell Medical College, New York, NY, and approved April 28, 2014 (received for review December 24, 2013)

Aging is associated with the accumulation of several types of damage: in particular, damage to the proteome. Recent work points to a conserved replicative rejuvenation mechanism that works by preventing the inheritance of damaged and misfolded proteins by specific cells during division. Asymmetric inheritance of misfolded and aggregated proteins has been shown in bacteria and yeast, but relatively little evidence exists for a similar mechanism in mammalian cells. Here, we demonstrate, using long-term 4D imaging, that the vimentin intermediate filament establishes mitotic polarity in mammalian cell lines and mediates the asymmetric partitioning of damaged proteins. We show that mammalian JUNQ inclusion bodies containing soluble misfolded proteins are inherited asymmetrically, similarly to JUNQ quality-control inclusions observed in yeast. Mammalian IPOD-like inclusion bodies, meanwhile, are not always inherited by the same cell as the JUNQ. Our study suggests that the mammalian cytoskeleton and intermediate filaments provide the physical scaffold for asymmetric inheritance of dynamic quality-control JUNQ inclusions. Mammalian IPOD inclusions containing amyloidogenic proteins are not partitioned as effectively during mitosis as their counterparts in yeast. These findings provide a valuable mechanistic basis for studying the process of asymmetric inheritance in mammalian cells, including cells potentially undergoing polar divisions, such as differentiating stem cells and cancer cells.

inclusion body | spatial quality control

Aging is universally associated with a global decline in cellular function (1–3). Due to the multiplicity of mechanisms that undergo aging-related dysfunction, its mechanistic basis, or "senescence factor," has been difficult to pinpoint. Several studies have provided key insight into the identities of senescence factors by studying the asymmetric segregation of damage in single-cell organisms that rejuvenate the emerging generation by preventing the inheritance of damaged factors such as DNA, lipids, and proteins (1, 4, 5). In particular, a number of seminal studies have demonstrated that bacteria and yeast use a complex and multifaceted machinery to prevent the inheritance of damaged and aggregated proteins by the new generation by restricting them to the older lineage during cell division (1, 6, 7).

Although the precise mechanism for asymmetric inheritance of aggregates has been a matter of much debate (1, 7), the emerging model is that the spatial arrangement of misfolded proteins into quality control-associated IB (inclusion body)-like structures plays an essential role in asymmetric inheritance (1, 7). A key property of some quality-control IBs and other IB-like structures, which allows the cell to retain them in a specific lineage during mitosis, is their association and interaction with cellular organelles and cytoskeleton. In bacteria, for example, aggregated proteins are collected at the old pole of a dividing cell (5). A similar mechanism has been proposed in fission yeast (8). In the budding yeast *Saccharomyces cerevisiae*, several detailed studies demonstrated interdependence between asymmetric inheritance and the maintenance of the actin cytoskeleton and, in particular, the polarisome complex, which anchors the actin cytoskeleton in the emerging bud (9). Compromising the architecture of the actin cytoskeleton, even for a single generation, leads to a decrease in the replicative lifespan of the emerging cells (4).

Yeast cells manage the triage of protein misfolding and aggregation by spatially partitioning subpopulations of misfolded proteins to several membrane-less cytosolic quality-control IBs (10, 11). Upon misfolding, substrates localize to transient stress foci (SFs), which concentrate chaperones, holdases, and disaggregases (7). SFs are dynamic IBs that form in response to acute stress and may participate in the triage decision of whether to refold, degrade, or aggregate misfolded proteins (7). As misfolded substrates accumulate, and especially in response to external stresses, they accumulate in two quality-control IBs: Proteins targeted for degradation are directed to the JUNQ compartment and proteins that are targeted for active aggregation are directed to an insoluble IPOD compartment (10). Recently, we have demonstrated a new vital role for these inclusions in asymmetric inheritance of aggregates (or spatial quality-control/replicative rejuvenation) in yeast (7). The IPOD and JUNQ are selectively retained in the mother cell during budding. This asymmetry is due to the fact that IPOD and JUNQ are tethered to organelles. Critically, proteins that were trapped in SFs, and therefore failed to migrate to IPOD or JUNQ in time for mitosis, were passed on to successive generations of daughter cells (7).

Although a similar replicative rejuvenation mechanism in multicellular organisms has been sought after for some time, only a few seminal studies have found evidence for asymmetric

Significance

We show, for the first time to our knowledge, that vimentin intermediate filaments establish mitotic polarity in dividing mammalian cell lines. By confining damaged, misfolded, and aggregated proteins in JUNQ inclusion bodies, vimentin mediates their asymmetric partitioning during division. We also, to our knowledge, provide the first direct evidence of active proteasomal degradation in dynamic JUNQ inclusion bodies. This work sheds light on an important rejuvenation mechanism in mammalian cells and provides new biological insight into the role of inclusion bodies in regulating aggregation, toxicity, and aging.

Author contributions: M.O., H.S., and D.K. designed research; M.O., H.S., R.B., J.T., W.Ś., S.P., T.A., A.-c.A., and N.E. performed research; R.L. contributed new reagents/analytic tools; M.O., H.S., and W.Ś. analyzed data; and M.O., H.S., and D.K. wrote the paper.

The authors declare no conflict of interest.

This article is a PNAS Direct Submission.

Freely available online through the PNAS open access option.

[1]M.O. and H.S. contributed equally to this work.

[2]To whom correspondence should be addressed. E-mail: dan@mail.huji.ac.il.

This article contains supporting information online at www.pnas.org/lookup/suppl/doi:10.1073/pnas.1324035111/-/DCSupplemental.

aggregate segregation during mammalian or *Drosophila* mitosis (12, 13, 14). The mechanism for directing misfolded proteins to different inclusions structures, however, appears to be at least partially conserved from yeast to mammals. In previous work, we have demonstrated the existence of distinct IBs in human cultured cells: a JUNQ-like IB and an IPOD-like IB (from here on JUNQ and IPOD) (15, 16). The JUNQ contains mobile aggregates and accumulates chaperones, such as Hsp70, and active proteasomes (15). The IPOD sequesters insoluble amyloid aggregates from the rest of the cytosol (15). In striking similarity to the yeast JUNQ, the properties of the mammalian JUNQ are highly sensitive to stress. Under low-stress conditions, the JUNQ is a dynamic liquid phase compartment with high-degradation capacity (11, 17). Increased exposure to misfolding stress or localization of disease-associated proteins to the JUNQ instead of the IPOD leads to the maturation of the JUNQ into a less dynamic solid phase compartment, inhibiting degradation and eventually killing the cell (15, 18).

We set out to examine the mechanism of mitotic inheritance of misfolded proteins and aggregates in mammalian cells. Using long-term 4D imaging (19), we demonstrate asymmetric inheritance of JUNQ IBs during mitosis. Although the IPOD, containing amyloidogenic proteins, is frequently inherited by the same cell as the JUNQ, it is sometimes misinherited. Similar to yeast, we observe SFs in mammalian cells, which fail to be retained asymmetrically. We show that the inheritance of the JUNQ is mediated by the association of the JUNQ with the cytoskeleton. The misfolded proteins in the JUNQ are confined by a network of vimentin intermediate filaments and sometimes also actin (20). Whereas in yeast the JUNQ and IPOD are both tethered to organelles, the mammalian IPOD does not appear to specifically associate with the cytoskeleton or the MTOC (Microtubule Organizing Center). Therefore, a critical difference between yeast and mammalian asymmetry mechanisms may be a reduced ability to maintain the partitioning of insoluble amyloid aggregates. Finally, we show that replicative rejuvenation may confer a slight fitness advantage, under certain conditions, on the daughter cell that fails to inherit a JUNQ. In addition to uncovering a novel replicative rejuvenation mechanism in higher eukaryotes, our study suggests that vimentin establishes an axis of mitotic polarity in mammalian cells.

Results

Vimentin JUNQs Are Functional Degradation Compartments That Contain Active Proteasomes. We set out to determine whether there is a general mechanism in mammalian cells for asymmetrically partitioning misfolded and aggregated proteins during mitosis. Although asymmetric inheritance was suggested for mammalian inclusions of polyglutamine Huntingtin (12), these inclusions are unique due to their large size and insolubility; therefore, it is not clear whether asymmetric inheritance of these inclusions among two symmetrically dividing cells is a regulated mechanism or a product of the bulky nature of the IBs. Mammalian IBs, also sometimes called aggresomes, were initially universally associated with the property of being perinuclear, staining with MTOC markers and ubiquitin, requiring microtubule polymerization for formation, and being surrounded by a "vimentin cage" (20). Since then, a number of studies have suggested that the process of spatial and functional architecture of IBs is at least as complex in mammalian cells as in yeast (15). Misfolded proteins with differing properties do not always localize to the same IB and require different signals for triage between degradation, aggregation, and autophagy pathways (21). In particular, in recent work, we examined the JUNQ IB, which colocalizes with Hsp70 and sHsps and contains proteasomes (15, 22). Coexpressing a toxic aggregation species [e.g., fALS-associated protein Superoxide Dismutase (SOD1G93A mutant)] decreased the mobility of soluble misfolded proteins, such as von Hippen-Lindau (VHL) protein, Ubc9ts, or luciferase in the JUNQ. Decreased mobility, in turn, led to increased toxicity and decreased turnover of misfolded VHL (15). In contrast, the IPOD appears to be a sequestration compartment lacking association with proteasomes and potentially serving a protective function (15).

The role of JUNQs in mediating quality control implied to us that they may also play a role in replicative rejuvenation by providing a platform for the cell to confine damaged proteins during division. Juxtanuclear IBs have long been hypothesized to be quality-control compartments (10, 15), based on their colocalization with quality-control components and their role in mediating aggregate toxicity (15), but direct evidence for a quality-control role has been lacking. We were intrigued by the idea that JUNQs may be active degradation centers for misfolded proteins. We therefore set out to study the long-term dynamics of JUNQ biogenesis and function. Our first striking observation was that a vimentin cage-like IB forms ahead of misfolded protein accumulation (Fig. 1*A* and Fig. S1*A*; and Movies S1 and S2 and Fig. 1*B*). All experiments were repeated in HEK, N2a, and CHO cells, yielding similar results. We observed vimentin JUNQ formation even in the absence of proteasome inhibition, especially pronounced in HEK cells (Fig. S1*B*). In CHO and N2a cells, mild proteasome inhibition yielded JUNQ formation with nearly 100% robustness. JUNQ formation was reversible, indicating a physiological property of vimentin (Fig. S1*C*). The formation of the JUNQ takes roughly eight times longer than the formation of IPOD, suggesting that the JUNQ is a dynamic structure that forms in response to the slow accumulation of misfolded protein (Fig. 1*C*, Fig. S1*D*, and Movie S1). To visualize misfolded protein substrates of the JUNQ, we used misfolded VHL tagged with the Dendra2 fluorophore and expressed from a strong promoter. VHL initially forms SFs, as observed in yeast (7),

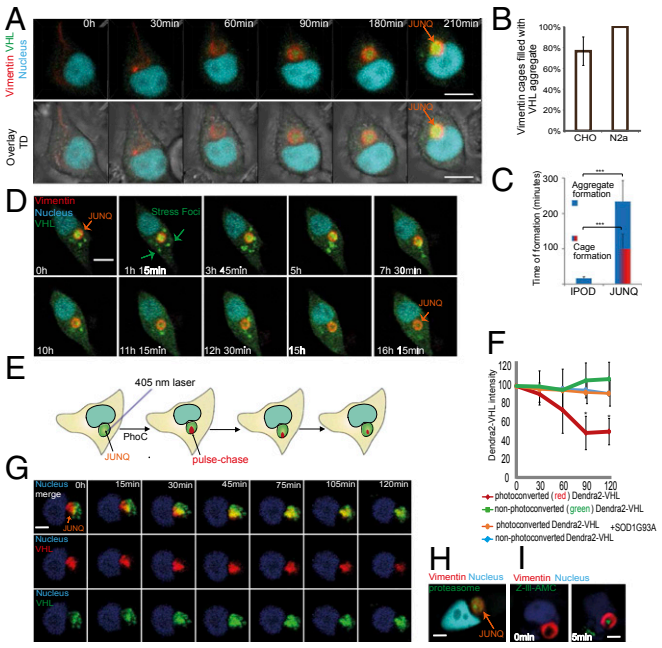

Fig. 1. Vimentin-enclosed JUNQs are transient compartments that degrade misfolded proteins. (*A*) Cells transfected with Vimentin-Orange2 and Dendra2-VHL, and treated with MG132 (4D live-cell imaging). (*B*) Percentage of cells containing a single aggregate surrounded by a vimentin cage. (*C*) Time required for IPOD and JUNQ formation. (*D*) VHL is degraded in the vimentin cage. VHL protein forms SFs, which are transported to JUNQ and then degraded. (*E*) Model of photoconversion. (*F* and *G*) A fraction of the JUNQ IB (~25%) was photoconverted to red (pulse), and the intensity of red/green fluorescence was monitored over time (chase) ($n = 20$). (*H*) Endogenously tagged proteasomes form domains within the vimentin cage. (*I*) Fluorescent reporter of proteasome activity, Z-Leu-Leu-Leu-AMC, was transfected into cells. Localization of active proteasomes was measured as increase of intensity of fluorescent signal over time. (Scale bar: 10 μm.)

which are transient (Fig. 1 *A* and *D* and Movie S2) and colocalize with Hsp70 (Fig. S1*A*). Over time, SFs are processed to form a single IB (Fig. 1 *A* and *D* and Fig. S1*A*). We observed consistent dynamic VHL IB formation (Fig. 1*A*), which we followed for up to 20 h using low laser power 3D time-lapse (Movies S1 and S2). In accordance with our hypothesis that JUNQs are degradation centers, we observed the appearance and disappearance of the VHL aggregate inside the vimentin cage, which persisted after all of the VHL was degraded (Fig. 1*D* and Movie S2) and disappears a few hours after proteasome inhibitor removal (Fig. S1*C*). Similar dynamics were observed for the recruitment of stress-induced Hsp70 into the vimentin JUNQ (Fig. S1*A*). These data suggest that the appreciable accumulation of substrate within JUNQ reflects a shifting balance between substrate delivery and degradation.

To verify that proteins were, in fact, being degraded by proteasomes inside the JUNQ, we used the photoconversion (PhoC) property of Dendra2, which allows for rapid, efficient, and irreversible conversion of the green form of Dendra2 to a red form, in a μm-sized region of interest in living cells, via a spatially restricted pulse of a 405-nm laser (Fig. 1*E*). This technique allowed us to follow a subpopulation of VHL over time, enabling a "pulse–chase" experiment in living cells. Red (PhoC) VHL inside JUNQ redistributed throughout the IB following PhoC, and disappeared within 2 h (Fig. 1 *F* and *G* and Movie S3), roughly corresponding to the previously characterized half-life of misfolded VHL (23). An additional pulse–chase of a smaller and more rapidly turned-over JUNQ is shown in Fig. S1*E*. We never observed an increase in cytosolic red signal, indicating that the PhoC VHL was degraded instead of being sent back to the cytosol. The level of green fluorescence remained relatively constant because de novo synthesis of VHL remained active. To compare the stability of proteins in the IPOD to those in the JUNQ, we expressed Dendra2-tagged polyglutamine Huntingtin (HttQ97). HttQ97 IPODs persisted indefinitely, and PhoC HttQ97 did not diffuse within the IB and was not degraded over the course of the experiment (Fig. S1 *F* and *G*). Interestingly, HttQ97 colocalized with heterologously expressed yeast prionogenic protein RNQ1 (Fig. S1*H*), suggesting a conserved mechanism for sequestering amyloidogenic proteins in the IPOD. In previous work (15), we hypothesized that amyloidogenic proteins (e.g., disease-associated SOD1G93A mutant) slow down degradation in the JUNQ when they accumulate there. The in vivo pulse–chase assay allowed us to test this hypothesis directly by measuring VHL turnover in a JUNQ with coaggregated SOD1G93A. In accordance with our previous observations, when SOD1G93A accumulated in the JUNQ with VHL, VHL was no longer turned over (Fig. 1*F*).

Using an endogenously tagged proteasome subunit (PSMB2-YFP) (24), we were able to observe endogenous proteasomes localizing to nanodomains within the JUNQ (Fig. 1*H*). To determine whether these proteasomes are functional, we transfected the cells with the fluorogenic proteasome substrate Z-III-AMC and observed the accumulation of fluorescent signal over time within the JUNQ (Fig. 1*I*). In contrast, the IPOD did not colocalize with proteasomes (Fig. S1*I*) (21). Together, these data establish a valuable approach to monitoring spatially confined misfolded protein degradation and demonstrate that JUNQ-localized proteasomes actively degrade spatially confined misfolded proteins. During low-stress conditions, the JUNQ is highly dynamic but converts to an aggregate state upon the accumulation of amyloidogenic proteins (15).

JUNQs Are Asymmetrically Segregated During Mitosis in Mammalian Cells. Following the formation and degradation of JUNQ over long periods of time allowed us to record many cell divisions. To our surprise, we observed remarkably consistent segregation of the JUNQ to a single cell following mitosis (nearly 100% robustness, $n > 100$ cells), (Fig. 2 *A*–*C* and Movies S4–S6). This phenomenon was observed regardless of whether the JUNQ contained VHL or the vimentin "cage" alone in the absence of VHL expression (Fig. 2 *B* and *C*). Interestingly, as in yeast, SFs formed by VHL failed to be segregated to a single cell along with the JUNQ (Fig. 2*B*).

Asymmetric segregation of IBs was demonstrated in previous studies, in particular using HttQ119 (12) (Fig. 2*D*), which forms insoluble IPODs (15). It was therefore important to determine whether the JUNQ and the IPOD were asymmetrically inherited via the same mechanism. Although it has previously been suggested that polyQ Htt forms perinuclear IBs that are caged by vimentin, similar to VHL, CFTR, and mutSod1 (12), we did not observe vimentin cages around the HttQ119 IB in live cells even when proteasome inhibitor treatment or misfolded protein expression triggers the formation of a vimentin cage elsewhere in the cell (Fig. 2*E* and Fig. S2*A*). The reason for this disparity may be an artifact of antibody immunofluorescence. PolyQ inclusions are broadly immunoreactive, and, when they are stained with anti-vimentin antibodies, there is a cage-like structure that is discernible (Fig. S2*B*) although, as shown in Fig. 2*E*, we detect no colocalization between vimentin and the IPOD with HttQ119.

Given that the IPOD and the JUNQ were spatially distinct, we then examined cell divisions in cells that contained both

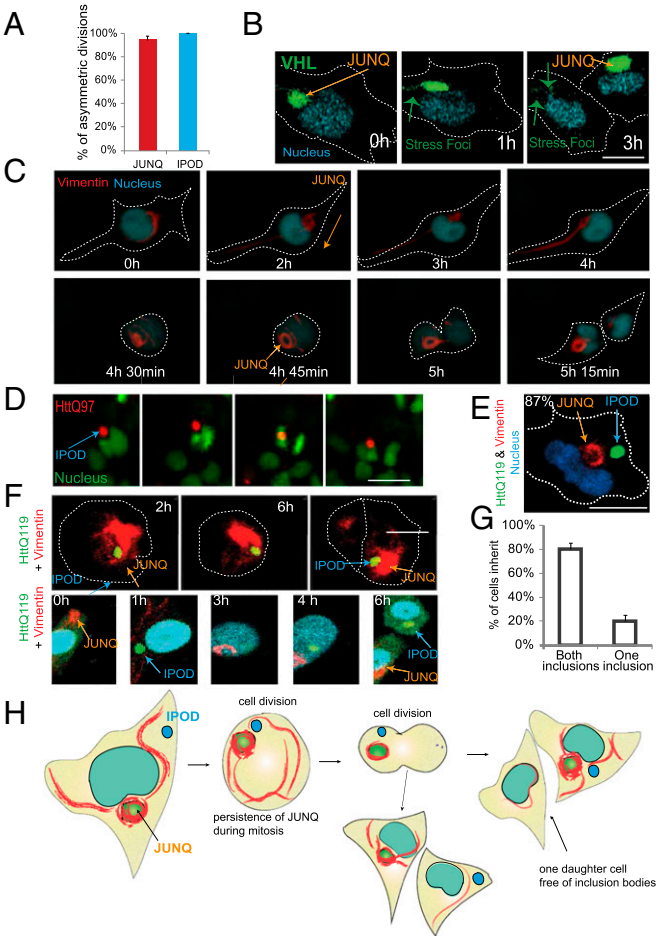

Fig. 2. Asymmetric inheritance of JUNQ and IPOD. (*A*) The number of asymmetric divisions of cells containing a single aggregate (IPOD or JUNQ) was quantified ($n = 42$ for JUNQ and $n = 35$ for IPOD). (*B*) An example of an asymmetric cell division with JUNQ marked by VHL. (*C*) A division of a cell with a vimentin JUNQ. (*D*) An asymmetric division of a cell containing IPOD marked by HttQ97. (*E*) Vimentin cage and IPOD are separate structures. (*F*) A cell division in which one cell inherits both vimentin JUNQ and IPOD (*Upper*) and a cell division where JUNQ and IPOD are inherited by different cells (*Lower*). (*G*) Quantification of *F* ($n = 29$). (*H*) A model of the asymmetric division of a cell with JUNQ and IPOD.

a vimentin cage/JUNQ and an HttQ119 IB. Although both inclusions were often retained in the same cell after mitosis (Fig. 2 *F*, *Upper*, *G*, and *H* and Movie S5), in roughly a fifth of the observed divisions, the JUNQ and the IPOD were inherited by different cells (Fig. 2 *F*, *Lower*, *G*, and *H* and Movie S6), in stark contrast to the yeast JUNQ and IPOD inclusions that are retained by the same cell in 100% of budding events (7).

Polyglutamine Huntingtin Inclusions Do Not Associate with Spindle Pole Body or the MTOC. The divergence between yeast and mammalian cells in inclusion inheritance prompted us to reexamine the localization of polyQ Htt inclusions in *S. cerevisiae*. Several studies have suggested that polyQ Htt inclusions colocalize with the spindle-pole body (SPB), the yeast functional homolog of the MTOC (25, 26). We have previously reported (10) that the polyQ Htt localizes to the IPOD and that the IPOD is tethered to the vacuole (7) and is therefore not in contact with the nucleus, much less the SPB. Without visualizing the nucleus of the cell, and without imaging the entire three dimensions of a yeast cell, which is a nearly perfect sphere, it is quite difficult to determine colocalization. Moreover, a recent study (26) demonstrated that RNQ1, another polyQ protein localizing to the IPOD, can recruit endogenous SPB components, such as Spc42, into the insoluble aggregate, suggesting that, in the study that reported HttQ97-SPB colocalization, coaggregation may have been interpreted as functional colocalization.

In light of this controversy and its potential relevance to the question of conservation of asymmetric inheritance pathways between yeast and mammals, we sought to examine the question of IPOD localization in yeast, vis-à-vis the SPB, using live cell 4D imaging. We expressed HttQ97 in yeast cells with fluorescent nuclei, vacuoles, and SPBs visualized via tagged Spc42 as in ref. 26 and tagged α-tubulin (Tub1). The live yeast were imaged in 3D at high temporal resolution. By visualizing all of the relevant yeast anatomy in the same cell, together with the IPOD, we can clearly conclude that the HttQ97 IPOD has no association with the SPB (Fig. 3 *A–D*) although, due to the small size of the yeast cell and its spherical structure, it can be mistakenly thought to colocalize with the SPB if imaged in 2D (Fig. 3 *C* and *E*). The JUNQ also exhibits no colocalization with the SPB (10). All of the imaged yeast were live and dividing (Fig. 3*D*), and hundreds of yeast were imaged. Similarly, in mammalian cells, in contrast to JUNQ (Fig. 3*F*, *Left*), the HttQ119 IPOD does not appear to be associated with the MTOC (Fig. 3*F*, *Right* and Fig. S2C).

The Mammalian JUNQ Is Physically Associated with the MTOC Whereas the IPOD Is Not. The lack of any association between yeast inclusions and the SPB caused us to examine the robustness of the association between mammalian inclusions and the MTOC. On one hand, early studies suggested that both vimentin-caged dynamic inclusions (containing CFTR or mutSod1) as well as polyQ Htt inclusions were perinuclear and colocalized with the MTOC (12). On the other hand, we have observed polyQ inclusions at arbitrary locations in the mammalian cell (10, 15). JUNQs are much more consistently perinuclear but do not always sit directly on top of the MTOC (Fig. S2 *C* and *D*). Moreover, looking along the *z* axis in a mammalian cell imaged in 3D (Fig. S2*E*), it is clear that, in most mammalian cells, much of the available cytosolic volume is perinuclear whereas most of the cell-surface area is at most a few micrometers thick. Perhaps mammalian inclusions are often perinuclear because that is where most of the cytosol is located? We devised a way of testing the robustness of the association between the inclusions and the MTOC using Nesprin 4 (27). Nesprin 4 is expressed in polarized cells and directs the movement of the MTOC away from the nucleus (Fig. 3*G* and Fig. S2*F*) (27). Ectopic expression of Nesprin 4 caused a dislocation of the vimentin JUNQ away from the nucleus, together with the MTOC (Fig. 3 *H–J*, Fig. S2 *G*, *H*, and *I*, and Movies S7–S9). These data assert that the JUNQ is functionally associated with the MTOC and suggest that this

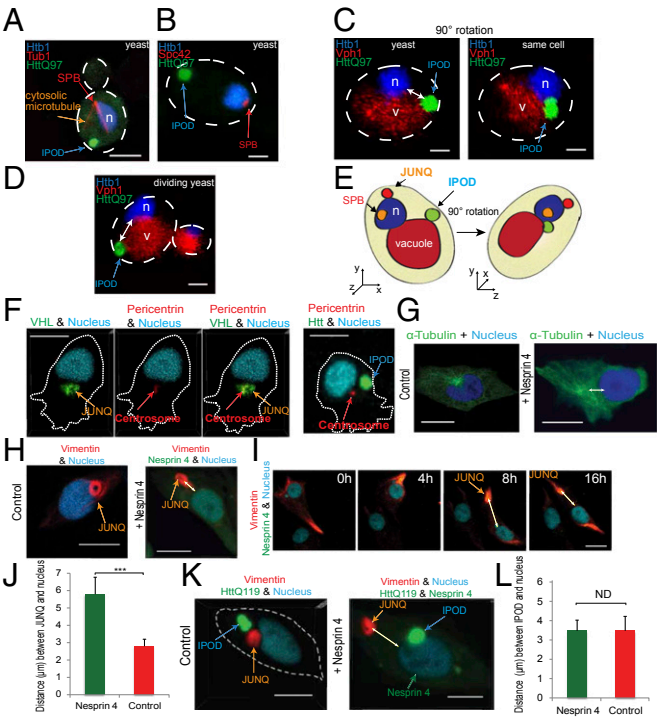

Fig. 3. The yeast IPOD is associated with the vacuole and not the SPB whereas the mammalian JUNQ, but not IPOD, is associated with MTOC. (*A*) Live yeast cells with tagged nucleus and tubulin, and expressing HttQ97, were imaged in 3D. (Scale bar: 1 μm.) (*B*) The SPB was visualized with tagged Spc42, in a live cell expressing HttQ97. (*C*) A 3D image of nucleus, vacuole, and IPOD (*Left*) and the same cell at a 90 degree angle (*Right*). (*D*) Dividing cell with nucleus, vacuole, and IPOD. (*E*) Model of *C*. (*F*) JUNQ with VHL colocalizes with centrosome. IPOD does not colocalize with centrosome. (*G*) Ectopic expression of Nesprin 4 causes relocation of centrosome. (*H* and *I*) Position of JUNQ in control and Nesprin 4-expressing cells. (*J*) The distance between the center of vimentin JUNQ and the nucleus in cells expressing Nesprin 4 vs. control (n = 22). (*K*) Position of JUNQ and IPOD in cells expressing Nesprin 4. (*L*) Distance between the IPOD and the nucleus.

association may be exploited by the cell to regulate the inheritance of misfolded proteins located in the JUNQ. Strikingly, even after division, cells expressing Nesprin 4 have a dislocated JUNQ (Movie S10). Using tagged pericentrin and α-tubulin, we verified that the JUNQ is being formed close to the MTOC (Fig. 3*F*), although not necessarily at the MTOC (Fig. S2*C*). Unlike the JUNQ, IPOD localization was completely unaffected by Nesprin 4 expression and MTOC displacement (Fig. 3 *K* and *L*). The IPOD remained at arbitrary localization relative to the nucleus in control cells (Fig. 3*K*, *Left*) and in Nesprin 4-expressing cells (Fig. 3*K*, *Right*). These data might explain the surprising observation in Fig. 2*F*, showing that the HttQ119 IPOD does not always segregate with the JUNQ. In contrast to JUNQ, which is associated with MTOC (Fig. 3*F*, *Left* and Fig. S2*D*), the IPOD does not appear to be associated with the MTOC (Fig. 3*F*, *Right*), nor with vimentin (Fig. 2*E*); therefore, the cell may be limited in its ability to control IPOD localization during mitosis. Our observation that the IPOD does nevertheless disproportionately partition together with the JUNQ (in 80% of cases) (Fig. 2*F*) suggests that there is some association between the IPOD and the cytoskeleton, albeit less robust than that of the JUNQ. This model is supported by data from Rujano et al., showing deposition of polyQ disease-associated proteins in intestinal crypt stem cells and dividing transit cells committed to differentiation (12). Together, these data lead to an intriguing conclusion: whereas in yeast dynamic aggregates and insoluble aggregates can easily be withheld from the emerging population by confinement to JUNQ and IPOD, mammalian cells are able

to spatially regulate the inheritance of the dynamic JUNQ with complete fidelity, but regulate the mitotic partitioning of amyloids in the IPOD much less robustly.

The Vimentin Intermediate Cytoskeletal Network Is Partitioned Asymmetrically During Mitosis. Whereas F-actin, mitochondria, and α-tubulin all partitioned symmetrically, vimentin demonstrated a nearly uniform polarity during mitosis (Fig. 4 *A*–*C* and Movie S11) with one of the daughter cells receiving a substantially smaller fraction of cellular vimentin (Fig. 4*C*). Although the vimentin JUNQ formed before mitosis and often dissociated after (Fig. 4*A*), and despite global cytoskeletal reorganization, the JUNQ vimentin structure remained intact throughout mitosis (Fig. 4 *A*, *B*, and *D*, Fig. 2*C*, and Movie S4). PhoC experiments showed that vimentin is a long-lived protein (Fig. S1*F*); therefore, the inherited vimentin is "old" and might therefore be a more general vehicle for asymmetric partitioning by defining polarity, and perhaps by physically retaining old or damaged cellular material. In support of this model, our time-lapse studies showed that roughly 50% of HEK cells (not expressing a misfolded substrate or treated with proteasome inhibitors) had a JUNQ at any given time (when we started imaging) whereas the other 50% formed a JUNQ just before mitosis (Fig. 4 *A*, *B*, and *E* and Fig. S3*A*). Together, our results point to a dual role for the JUNQ: degrading misfolded proteins and mediating their asymmetric inheritance during mitosis.

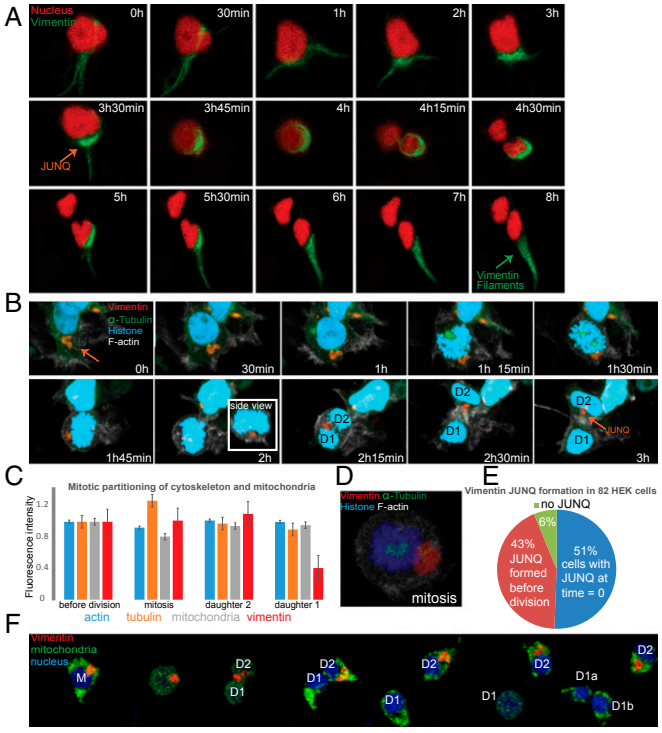

Fig. 4. The vimentin intermediate cytoskeletal network is partitioned asymmetrically during mitosis and confers slight fitness advantage on cells failing to inherit a JUNQ. (*A*) Vimentin forms a JUNQ before mitosis, is partitioned asymmetrically, and then returns back to fibrilar vimentin. (*B*) Vimentin is partitioned asymmetrically whereas tubulin and actin are not. (*C*) Quantification of actin, tubulin, mitochondria, and vimentin partitioning during mitosis ($n = 36$). (*D*) JUNQ remains intact during mitosis. (*E*) JUNQ formation dynamics were quantified in 82 HEK cells. (*F*) Cells were followed through two mitoses. Cells that failed to inherit a JUNQ in the first mitosis (D1) divided sooner than their sister cells that did inherit a JUNQ (eight out of eight two-generation cell divisions). Mitochondria marked with Mito-Dendra2 were inherited symmetrically. Experiments were performed on HEK cells without MG132 treatment.

Replicative Rejuvenation Confers a Slight Fitness Advantage onto Cells That Fail to Inherit a JUNQ. Using extremely long 3D time-lapse studies, over the course of 3–4 d, we were able to observe multiple generations of HEK cell divisions. We first wanted to determine whether the asymmetric partitioning of vimentin JUNQs correlated with asymmetric inheritance of old versus new mitochondria (similarly to what has been shown in yeast) (28). We therefore undertook four-color live-cell imaging of cells expressing far-blue vimentin and far-red nucleus, together with mito-Dendra2. We photoconverted whole-cell mitochondria and followed divisions. Following successive mitoses demonstrated no asymmetry between cells inheriting the JUNQ and JUNQ-free daughter cells, with respect to inheritance of new (blue) versus old (red) mitochondria (Fig S3*B*). We then asked whether inheriting or failing to inherit a JUNQ nevertheless confers any advantage on the daughter cells. In every second-generation division that we were able to track, the cell that failed to inherit a JUNQ divided several hours sooner than its sister cell that inherited the JUNQ (Fig. 4*F* and Movie S12). This observation may suggest that withholding of JUNQ substrates through the replicative rejuvenation process eases the proteostasis burden on the noninheriting cells, thus giving certain cells a fitness advantage.

Discussion

This study set out to investigate the role of IBs in replicative rejuvenation and asymmetric inheritance of damaged proteins. Although IBs were suspected of mediating misfolded protein degradation due to association with ubiquitin, proteasomes, and lysosomes (21, 29), little direct evidence existed for degradation within the IB, as opposed to clearance from the IB by diffusion followed by degradation elsewhere. Our 3D longitudinal experiments demonstrate protein turnover in the JUNQ. Our 4D imaging allows us to monitor different subpopulations of proteins in the cell and to track small transient structures during cell division. Additionally, we demonstrate that the JUNQ is asymmetrically inherited, providing a basis for further study of how damaged cellular material is partitioned during division. Direct observation of misfolded protein turnover in IBs reinforces the predictions of many studies (15, 29) suggesting that inclusions are not passive by-products of protein aggregation, but rather serve an important quality-control function in the cell. Seeing JUNQ formation and maturation as a dynamic process helps to reconcile divergent observation into a coherent model. We propose that JUNQ inclusions can form in many cell types, but they are easily detectable when a sufficient load of misfolded proteins accumulates to necessitate the proliferation of a visible vimentin JUNQ structure. In certain cell lines, such as HEK cells, large JUNQ IBs form in nearly every cell, especially before cell division. In other cell lines, such as N2a and CHO cells, spontaneous JUNQ formation is less apparent in unperturbed cells, but proteasome inhibition or expression of high levels of misfolded proteins leads to the appearance of visible JUNQs. We hypothesize that these differences reflect variability in basal levels of misfolded proteins in different cell lines and that whether a JUNQ is highly visible, or requires proteasome inhibition to become apparent, is akin to a traffic jam, which can form as a result of an overabundance of proteins trafficked to the JUNQ for degradation, or an impairment of its degradation capacity. Over time, under stress and accumulating levels of misfolded proteins, the JUNQ transitions from a dynamic liquid-phase compartment to an insoluble solid-phase compartment that is no longer capable of efficient protein turnover by the proteasome. We suggest that this transition also takes place in cases of disease-associated proteins. In its immobile form, the JUNQ sequesters chaperones, such as Hsp70 (15). This model of JUNQ maturation into an "aggresome" is particularly in line with several recent studies demonstrating directed transport of lysosomes to IBs via vimentin and actin (30, 31) and the clearance of IBs by lysosomal degradation (29, 32). Looking at hundreds of cells, we noticed that vimentin was a tubular clump in some cells and adopted more of a ring-like shape as the JUNQ

became bigger. This change in the shape of the JUNQ coincided with the recruitment of F-actin to the JUNQ (Fig. S3*C*), perhaps as a means of transporting lysosomes to the compartment. Once the misfolded proteins in the JUNQ begin to aggregate and the JUNQ loses its quality-control capacity, lysosomes may have to be brought in as a last resort. Perhaps this mode of JUNQ function is the default in postmitotic cells, which are unable to use replicative rejuvenation as a form of quality control.

The mechanism responsible for selective association of JUNQ with one daughter cell after division remains to be determined. One interesting possibility is that mammalian cell divisions are actually polar and divide into two cells: one containing specific old material and one containing specific new material. It has been suggested that old centrosomes and other cellular components are inherited asymmetrically, and intermediate filaments may similarly be key regulators of polarity in mammalian cells. Interestingly, we have gathered preliminary evidence suggesting that avoiding JUNQ inheritance provides a slight fitness advantage, enabling the JUNQ-free daughter cell to divide before the JUNQ-inheriting sister. It is interesting to speculate that, by mediating the polarity of divisions, vimentin may be a regulator of aging. Because vimentin interacts with actin, tubulin, and membranes, it might thus play a role in mediating the inheritance of cellular material during division. Cellular levels of vimentin increase upon treatment with proteasome inhibitors (Fig. S3*D*), perhaps to more effectively partition misfolded proteins. Therefore, the JUNQ may be retained by the daughter cell destined to inherit other old cellular material. This model would explain the apparent fitness cost for inheriting the JUNQ. Alternatively, even if the division is asymmetric only with respect to the JUNQ, the decrease in division rate might be the result of inheriting a higher load of misfolded proteins. Under certain circumstances, however, JUNQ inheritance may also be beneficial because chaperones and proteasomes are also highly enriched in the JUNQ and therefore the inheriting cells receive more quality-control factors. Given our previous observation that the JUNQ can mature from a dynamic quality-control structure to a source of toxicity and aggregation, the ability to control mitotic inheritance of the JUNQ may be crucial for multicellular systems. Our data also raise the surprising possibility that the insoluble IPOD can sometimes evade the spatial quality-control mechanism in mammalian cells.

Emerging evidence suggests that spatial quality control and replicative rejuvenation are essential components of homeostasis in single cells and multicellular organisms (1). It appears that, in multicellular organisms, replicative rejuvenation and the chronological lifespan of cells, as opposed to cell-type, determine the level of damaged and misfolded proteins present in the cell (14). Thus, the mechanisms regulating replicative rejuvenation may be the key to understanding the highly divergent susceptibility of different tissues to aggregate toxicity. Our study provides the basis to explore the molecular mechanism governing replicative rejuvenation in mammalian cells and provides markers for examining many facets of asymmetry in living cells, including in stem cells and cancer cells, that can undergo polar divisions.

Methods

For time-lapse imaging, we used a dual point-scanning Nikon A1Rsi microscope equipped with a Piezo stage. Cells were cultured and transfected according to standard protocols. Detailed materials and methods can be found in *SI Methods*.

ACKNOWLEDGMENTS. We thank Ehud Cohen, Jeremy England, Maya Schuldiner, Mark Kaganovich, and members of the D.K. laboratory for valuable comments. We thank Ariel Stanhill for his generous gift of CHO cells with integrated PSMD14-YFP. We thank P. Golik, E. Bartnik, Ł. Borowski, A. Chlebowski, P. Mulica, A. Taracha, A. Socha, M. Aleksander, A. Kołodziejczyk, and A. Sobolewska for valuable discussion and technical support. M.O., H.S., J.T., and W.Ś. were partially supported by the Foundation U. Varsoviensis and Rada Konsultacyjna UW. The research leading to these results has received funding from the European Research Council under the European Union's Seventh Framework Programme (FP/2007-2013)/ERC-StG2013 337713 DarkSide starting grant. This work was also supported by Israel Science Foundation Grant ISF 843/11, German Israel Foundation Grant GIF I-1201-242.13/2012, an Israel Health Ministry grant under the framework of E-Rare-2, a Niedersachsen-Israel Research Program grant, and a grant from the American Federation for Aging Research.

1. Nyström T, Liu B (2014) The mystery of aging and rejuvenation-a budding topic. *Curr Opin Microbiol* 18C:61–67.
2. Denoth Lippuner A, Julou T, Barral Y (2014) Budding yeast as a model organism to study the effects of age. *FEMS Microbiol Rev* 38(2):300–325.
3. Henderson KA, Gottschling DE (2008) A mother's sacrifice: What is she keeping for herself? *Curr Opin Cell Biol* 20(6):723–728.
4. Aguilaniu H, Gustafsson L, Rigoulet M, Nyström T (2003) Asymmetric inheritance of oxidatively damaged proteins during cytokinesis. *Science* 299(5613):1751–1753.
5. Lindner AB, Madden R, Demarez A, Stewart EJ, Taddei F (2008) Asymmetric segregation of protein aggregates is associated with cellular aging and rejuvenation. *Proc Natl Acad Sci USA* 105(8):3076–3081.
6. Erjavec N, Cvijovic M, Klipp E, Nyström T (2008) Selective benefits of damage partitioning in unicellular systems and its effects on aging. *Proc Natl Acad Sci USA* 105(48): 18764–18769.
7. Spokoini R, et al. (2012) Confinement to organelle-associated inclusion structures mediates asymmetric inheritance of aggregated protein in budding yeast. *Cell Rep* 2(4):738–747.
8. Coelho M, et al. (2013) Fission yeast does not age under favorable conditions, but does so after stress. *Curr Biol* 23(19):1844–1852.
9. Liu B, et al. (2010) The polarisome is required for segregation and retrograde transport of protein aggregates. *Cell* 140(2):257–267.
10. Kaganovich D, Kopito R, Frydman J (2008) Misfolded proteins partition between two distinct quality control compartments. *Nature* 454(7208):1088–1095.
11. Alberti S (2012) Molecular mechanisms of spatial protein quality control. *Prion* 6(5): 437–442.
12. Rujano MA, et al. (2006) Polarised asymmetric inheritance of accumulated protein damage in higher eukaryotes. *PLoS Biol* 4(12):e417.
13. Fuentealba LC, Eivers E, Geissert D, Taelman V, De Robertis EM (2008) Asymmetric mitosis: Unequal segregation of proteins destined for degradation. *Proc Natl Acad Sci USA* 105(22):7732–7737.
14. Bufalino MR, DeVeale B, van der Kooy D (2013) The asymmetric segregation of damaged proteins is stem cell-type dependent. *J Cell Biol* 201(4):523–530.
15. Weisberg SJ, et al. (2012) Compartmentalization of superoxide dismutase 1 (SOD1G93A) aggregates determines their toxicity. *Proc Natl Acad Sci USA* 109(39): 15811–15816.
16. England JL, Kaganovich D (2011) Polyglutamine shows a urea-like affinity for unfolded cytosolic protein. *FEBS Lett* 585(2):381–384.
17. Weber SC, Brangwynne CP (2012) Getting RNA and protein in phase. *Cell* 149(6): 1188–1191.
18. Oling D, Eisele F, Kvint K, Nyström T (2014) Opposing roles of Ubp3-dependent deubiquitination regulate replicative life span and heat resistance. *EMBO J* 33(7): 747–761.
19. Spokoini R, Shamir M, Keness A, Kaganovich D (2013) 4D imaging of protein aggregation in live cells. *J Vis Exp*, 10.3791/50083.
20. Johnston JA, Ward CL, Kopito RR (1998) Aggresomes: A cellular response to misfolded proteins. *J Cell Biol* 143(7):1883–1898.
21. Zhang X, Qian SB (2011) Chaperone-mediated hierarchical control in targeting misfolded proteins to aggresomes. *Mol Biol Cell* 22(18):3277–3288.
22. Ben-Gedalya T, et al. (2011) Cyclosporin-A-induced prion protein aggresomes are dynamic quality-control cellular compartments. *J Cell Sci* 124(Pt 11):1891–1902.
23. McClellan AJ, Scott MD, Frydman J (2005) Folding and quality control of the VHL tumor suppressor proceed through distinct chaperone pathways. *Cell* 121(5):739–748.
24. Stanhill A, et al. (2006) An arsenite-inducible 19S regulatory particle-associated protein adapts proteasomes to proteotoxicity. *Mol Cell* 23(6):875–885.
25. Wang Y, et al. (2009) Abnormal proteins can form aggresome in yeast: Aggresome-targeting signals and components of the machinery. *FASEB J* 23(2):451–463.
26. Treusch S, Lindquist S (2012) An intrinsically disordered yeast prion arrests the cell cycle by sequestering a spindle pole body component. *J Cell Biol* 197(3):369–379.
27. Roux KJ, et al. (2009) Nesprin 4 is an outer nuclear membrane protein that can induce kinesin-mediated cell polarization. *Proc Natl Acad Sci USA* 106(7):2194–2199.
28. Vevea JD, Swayne TC, Boldogh IR, Pon LA (2014) Inheritance of the fittest mitochondria in yeast. *Trends Cell Biol* 24(1):53–60.
29. Zaarur N, et al. (2014) Proteasome failure promotes positioning of lysosomes around the aggresome via local block of microtubule-dependent transport. *Mol Cell Biol* 34(7):1336–1348.
30. Styers ML, et al. (2004) The endo-lysosomal sorting machinery interacts with the intermediate filament cytoskeleton. *Mol Biol Cell* 15(12):5369–5382.
31. Toivola DM, Tao GZ, Habtezion A, Liao J, Omary MB (2005) Cellular integrity plus: Organelle-related and protein-targeting functions of intermediate filaments. *Trends Cell Biol* 15(11):608–617.
32. Lee JY, et al. (2010) HDAC6 controls autophagosome maturation essential for ubiquitin-selective quality-control autophagy. *EMBO J* 29(5):969–980.

Supporting Information

Ogrodnik et al. 10.1073/pnas.1324035111

SI Methods

Confocal 3D Time-Lapse: 4D Imaging. For time-lapse imaging, we used a dual point-scanning Nikon A1R-si microscope equipped with a PInano Piezo stage, using a 60× PlanApo IR water objective NA 1.27, 0.3-μm slices, and 0.2–2% laser power (from 65-mW 488-nm laser and 50-mW 561-nm laser) to acquire 3D movies. Images were acquired in resonant-scanning or galvano-scanning mode, and *Z* stacks were acquired every 15 min for 6 h or every 30 min for 12–48 h. Each *Z* series was acquired with 0.5- to 1-μm step size and 10–35 steps. Volume-view snapshots from movies are shown in Figs. 1, 2, and 4, Figs. S1–S3, and in Movies S1–12.

Photoconversion Assay. Dendra2-von Hippen-Lindau (VHL) and HttQ97-Dendra2 IBs (inclusion bodies) were partly photoconverted (~25% area of the IB) via a spatially restricted pulse of a 405-nm laser. Images were collected every 15 min as described in the 4D imaging section. Fluorescence intensity (mean intensity) of photoconverted (red) and nonphotoconverted (green) aggregates was measured using ImageJ software. The rate of protein degradation is shown as a percentage of the intensity from the first time point.

Endogenous Proteasome Tagging. For generating CHO cells with genomically integrated proteasome substrates (which were a gift from Ariel Stanhill, Technion-Israel Institute of Technology, Haifa, Israel), plasmids carrying the specific proteasomal subunit fused to YFP were created by substituting the GST fusion of the respective plasmid (1). CHO cells were transfected with pCFL PSMB2-YFP, PSMD14-YFP, or YFPplasmids, and individual stable clones harboring fully integrated labeled subunits based on their ability to migrate in a 10–40% glycerol gradient only in proteasomal fractions were chosen.

Cell Culture and Transient Transfections. Chinese Hamster Ovary (2), mouse neuroblastoma Neuro 2A (N2a), and Human Embryonic Kidney 293 (HEK) were cultured in high-glucose DMEM (Sigma) supplemented with 50 mL/500 mL FBS (Sigma), 2 mM glutamine, 100 units/mL penicillin, and 100 μg/mL streptomycin (Invitrogen). Cultures were maintained at 37 °C and 5% CO_2 in a humidified incubator. For transient transfections, cells were grown to 50–60% confluence in round glasses (Ibidi) for time-lapse imaging. Cells were transfected using TransIT (Mirus) according to the manufacturer's instructions. Cells were treated with 2 μM or 5 μM MG132 (or DMSO control) 48 h after transfection for 2 h or 6 h, and then media was changed. Treatment with higher concentration of MG132 (5 μM) was used to elicit the maximum number of cells with inclusions for the aggregate formation whereas, for asymmetry distribution experiments, very mild treatments (2 μM MG132, 2 h for N2a and CHO cells) or no treatment (for HEK cells) was used.

Plasmids. For transient transfection of mammalian cells, we used the plasmid pHttQ119-EYFP (enhanced yellow fluorescent protein), which drives the expression of a fragment of exon-1 of human Huntingtin fused to EYFP, which was kindly provided by Harm H. Kampinga (University of Groningen, Groningen, The Netherlands), pVimentin-PSmOrange2 driving the expression of human vimentin (kindly provided by Vladislav V. Verkhusha, Albert Einstein College of Medicine, Bronx, NY), pVimentin-tagBFP2 (kindly provided by Michael W. Davidson, Florida State University, Tallahassee, FL), pEGFP-C1-GFP-Nesprin 4 (a gift from Brian Burke, University of Florida, Gainesville, FL), RFP-pericentrin (a gift from Sean Munro, Medical Research Council, Cambridge, UK), and pEYFP-N1-HSP70 plasmid (provided by Richard Morimoto, Northwestern University, Evanston, IL). pDendra2-VHL, pDendra2-HttQ97, and pDendra2-α-Tubulin were generated by subcloning VHL and α-Tubulin into the pDendra2 vectors. NLS-iRFPx2 was generated by subcloning SV40 NLS and iRFP into pcDNA3.1. Mito-Dendra2 was generated by cloning the subunit VIII of cytochrome C into the pDendra2 vector. pCMVLifeAct-GFP plasmid was purchased from Ibidi.

Proteasome Function Assay. Localization of active proteasomes was assessed by measuring the increase of blue-channel fluorescence after addition of fluorogenic proteasome substrate 1, Z-Leu-Leu-Leu-AMC, (Sigma) in DMSO at a final concentration of 40 μM. Cells were used for imaging after 5 min of incubation. DMSO was added as a control. Each z-series was acquired with 1-μm step size and 15 total steps in galvano scanning mode. Image processing was performed using NIS-Elements software.

Immunofluorescence. Cells were grown on glass coverslips for 24 h and then transfected with HttQ119-YFP. After transfection, cells were incubated for 24 h and then washed three times with PBS and fixed with 3.7% formaldehyde for 15 min. Cells were permeabilized with 0.5% Triton X-100 in 10% FBS/PBS for 15 min. Cells were blocked with 10% FBS solution in PBS for 30 min. Cells were incubated with anti-vimentin antibody (dilution 1:200) (Santa Cruz) for 1 h. After three washes with PBS, secondary antibodies conjugated with Alexa Fluor 555 (Molecular Probes) were applied at 1:1,000 for 1 h. Cells were incubated for 5 min with Hoechst (1 mg/mL in PBS) and washed three times with PBS. Cells were mounted in ProLong Gold anti-fade reagent (Invitrogen).

Western Blot. Whole-cell protein was extracted from HeLa and MEF cell lines according to the standard protocols. PVDF membranes were incubated with the primary antibody anti-vimentin (1:200; Santa Cruz Biotechnology). The protein level was detected with a FujiFilm LAS-4000 CCD camera system.

Yeast Strains and Materials. Yeast media preparation and growth and yeast transformations were performed according to standard protocols as described previously (3). HttQ97-GFP was expressed under the control of a galactose-regulated promoter (Gal1p). The strains were grown to OD600 0.8 in synthetic media containing 2% raffinose for 72 h, diluted to OD600 0.2 in 2% galactose-containing media, and grown for 8 h. To shut off expression, galactose-containing media was replaced with synthetic media supplemented with 2% glucose (SD). Endogenously tagged strains were generated as described previously (3); TagBFP-tagged Htb1 strain was a gift from Simon Alberti (Max Planck Institute of Molecular Cell Biology and Genetics, Dresden, Germany).

Statistical Analysis. Data were checked for normality using the Shaprio–Wilk test. For Gaussian distribution, data were evaluated using the two-tailed, unpaired Student *t* test with Welch's correction. For non-Gaussian distribution, data were evaluated using the two-tailed Mann–Whitney test. For binary results, the data were evaluated using a two-tailed χ^2 test.

***P* Values for Data Shown in Figs. 1 and 4 and Fig. S3.** *P* values for data shown in Figs. 1 and 4 and Fig. S3 are as follows: *P* (vimentin cage vs. IPOD formation) ≤ 0.0001 (Student *t* test); *P* (JUNQ vs. IPOD formation) ≤ 0.0001 (Student *t* test); *P* (green vs. red fluorescence) = 0.0218, 0.0237, 0.0023 (Student *t* test); *P* (Nesprin 4 vs. control for JUNQ) ≤ 0.0001 (Mann–Whitney test); *P* (Nesprin 4 vs. control for IPOD) = 0.2694 (Mann–Whitney test); and *P* (JUNQ vs. IPOD) ≤ 0.0001 (χ^2 test).

1. Stanhill A, et al. (2006) An arsenite-inducible 19S regulatory particle-associated protein adapts proteasomes to proteotoxicity. *Mol Cell* 23(6):875–885.
2. Schoenfeld AR, Davidowitz EJ, Burk RD (2000) Elongin BC complex prevents degradation of von Hippel-Lindau tumor suppressor gene products. *Proc Natl Acad Sci USA* 97(15):8507–8512.
3. Spokoini R, et al. (2012) Confinement to organelle-associated inclusion structures mediates asymmetric inheritance of aggregated protein in budding yeast. *Cell Rep* 2(4):738–747.

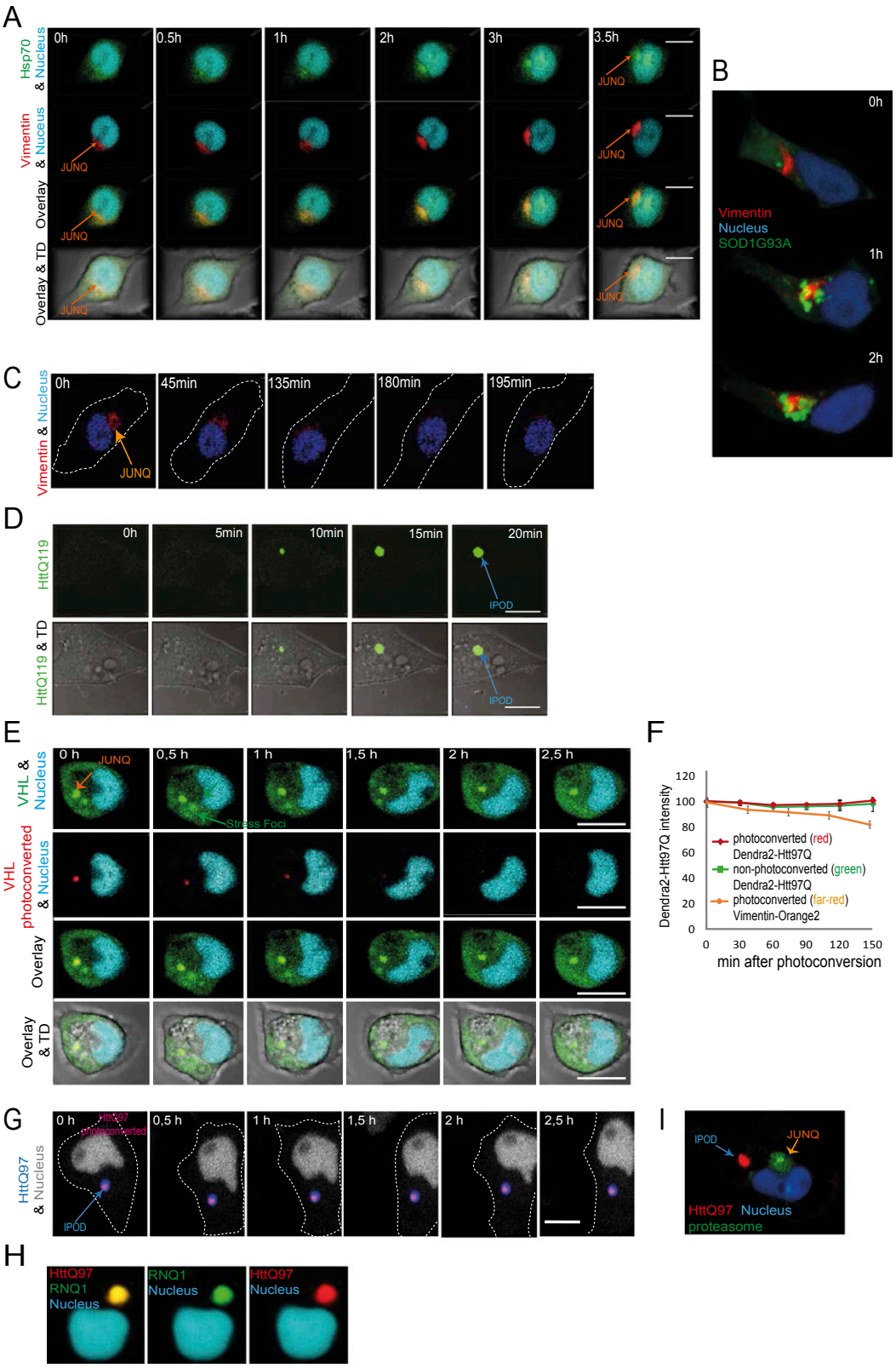

Fig. S1. (*A*) The Hsp70 stress-induced chaperone localizes inside vimentin JUNQ. (*B*) Formation of vimentin cage and JUNQ marked with SOD1G93A in the absence of MG132. (*C*) After removal of MG132, vimentin filaments redistribute throughout the cell. (*D*) The rapid process of IPOD formation. (*E*) Example of JUNQ pulse–chase with rapid turnover dynamics. (*F*) Quantitative analysis of IPOD (HttQ97) and vimentin photoconversion assay. The mean from three experiments, 10 cells per experiment is presented. (*G*) Red (photo-converted) HttQ97 protein is stable and immobile in IPOD. (*H*) Colocalization of Htt97Q with RNQ1 in IPOD. (*I*) Endogenously tagged proteasome subunits (PSMB2-YFP and PSMD14-YFP) do not colocalize with IPOD marked by pHtt97Q. (Scale bar: 10 μm for all supplementary figures.)

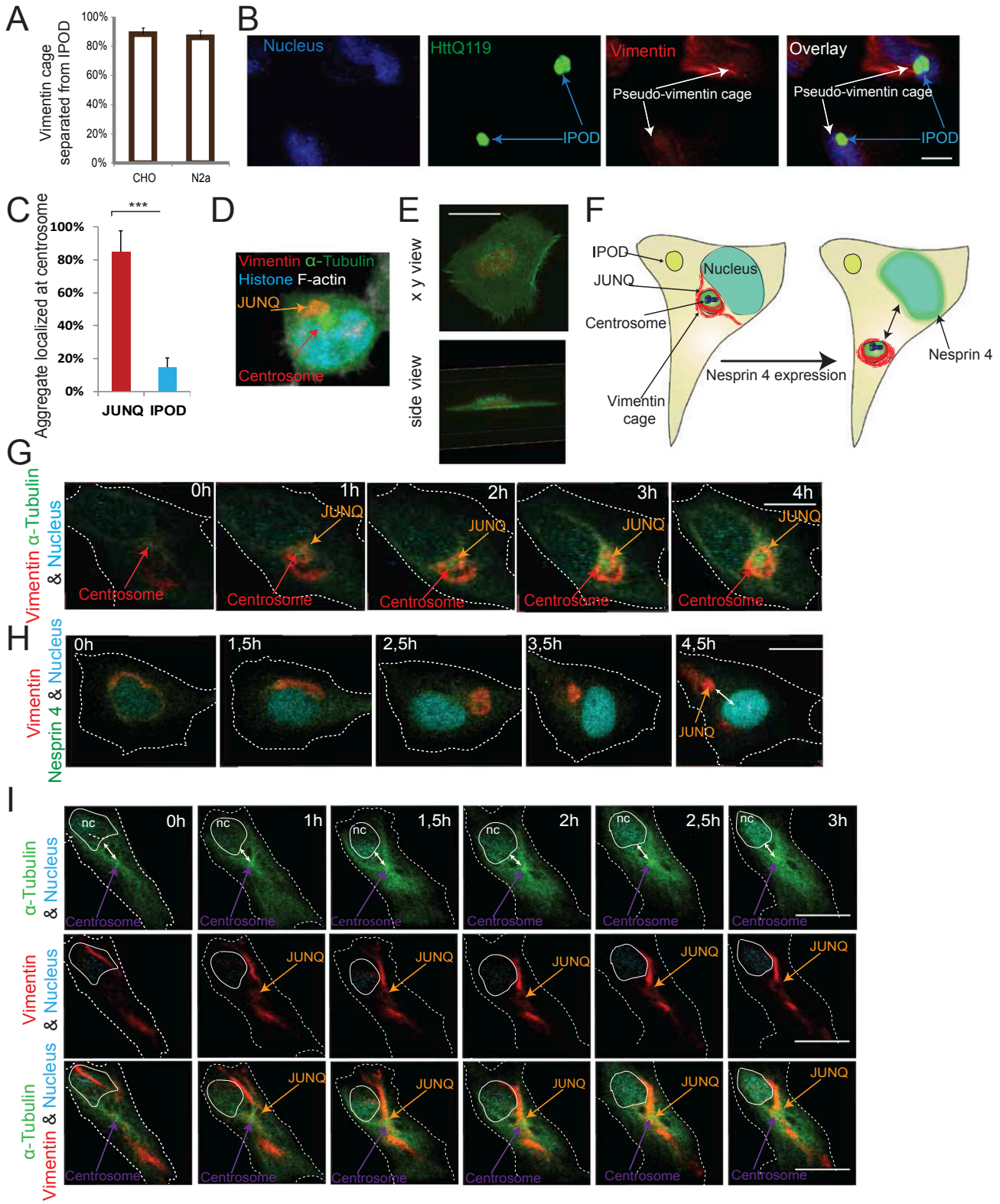

Fig. S2. (*A*) Quantitative analysis of the incidence of the vimentin cage spatially separated from IPOD. The experiment was repeated three times and at least 100 cells were counted per experiment. (*B*) Vimentin displacement caused by the presence of IPOD resembles vimentin cage. Cells expressing the pHttQ119-EYFP construct were fixed and vimentin and visualized by immunofluorescence. (*C*) The quantification of JUNQ marked with Dendra2-VHL and IPOD colocalization with centrosome marked by RFP-pericentrin. The experiments were repeated three times, and at least 21 cells were counted. (*D*) JUNQs are perinuclear but do not always sit directly on top of the MTOC (Microtubule Organizing Center). (*E*) Cell transfected with pCMVLifeAct-GFP from *x-y* view and side view. (*F*) A model presenting the position of JUNQ far from the nucleus in cells expressing Nesprin 4 and the IPOD position not affected by artificial cell polarization. (*G*) The process of vimentin cage formation at the centrosome marked by Dendra2-α-Tubulin (Movie S7). (*H*) Cells expressing Nesprin 4 form JUNQ marked by vimentin and move it far from the nucleus (Movie S8). (*I*) In cells expressing Nesprin 4, the MTOC is positioned far from the nucleus, and the vimentin cage is formed there as well.

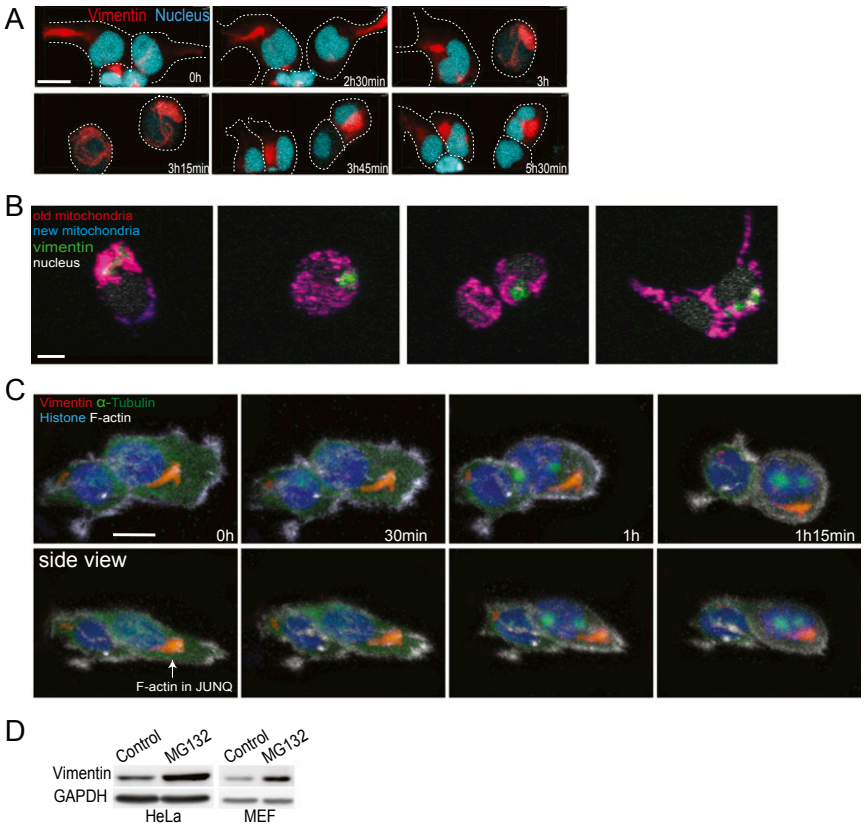

Fig. S3. (*A*) An example of JUNQ formation in two cells before mitosis followed by asymmetric partitioning of the intact JUNQ IB. (*B*) New (blue) and old (red) mitochondria are inherited symmetrically in HEK cells during division. Mito-Dendra2 was photoconverted after mitosis and cells were imaged until after mitosis. (*C*) In larger JUNQs, F-actin colocalization is often observed before cell division. (*D*) Western blot against vimentin showing an increase in vimentin levels upon proteasome inhibition with 10 μM MG132 for 2 h followed by protein extraction with Nonidet P-40, 0.1% buffer, and SDS/PAGE.

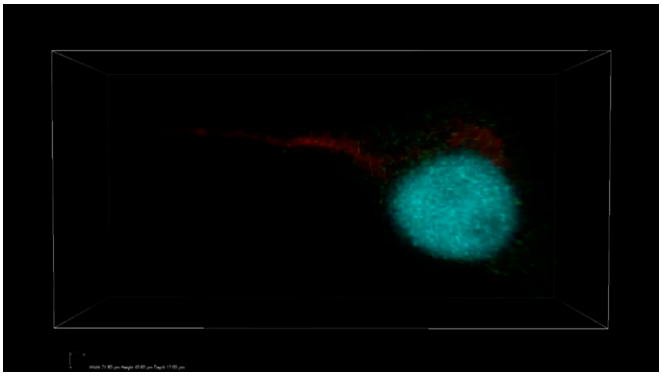

Movie S1. The formation of the vimentin/VHL JUNQ IB. Cells were transfected with Vimentin-mOrange2, NLS-iRFP, and pDendra2-VHL. Cells were treated with 5 μM MG132.

Movie S1

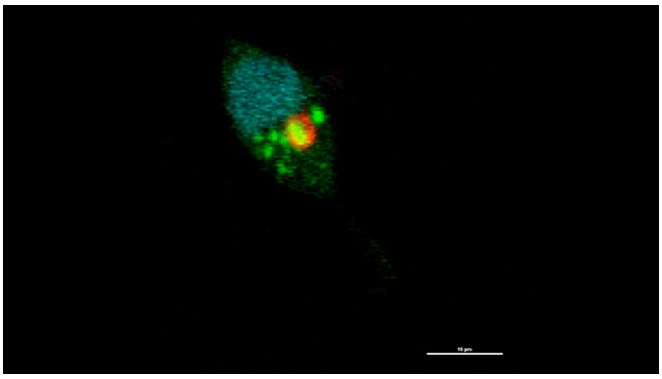

Movie S2. Clearance of JUNQ-like IB inside the vimentin JUNQ. Cells were transfected with Vimentin- mOrange2, NLS-iRFP, and pDendra2-VHL. Cells were treated with 5 μM MG132 for 2 h, and then MG132 was washed out.

Movie S2

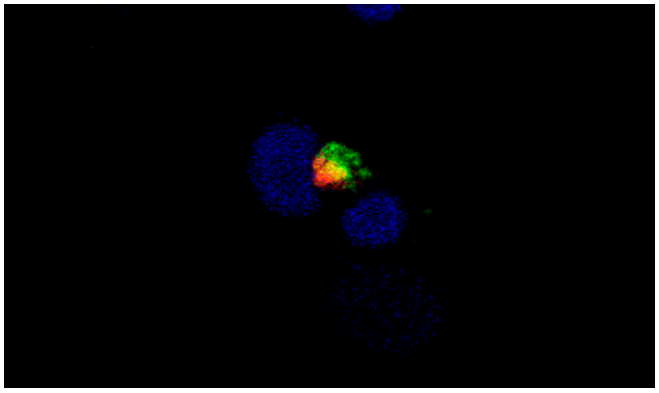

Movie S3. Degradation of VHL protein inside JUNQ. Cells were transfected with pDendra2C-VHL and NLS-iRFP. Cells were treated with 2 μM MG132 for 5 h, and then MG132 was washed out. A 405-nm laser was used to photoconvert a part of JUNQ-like IB from green to red.

Movie S3

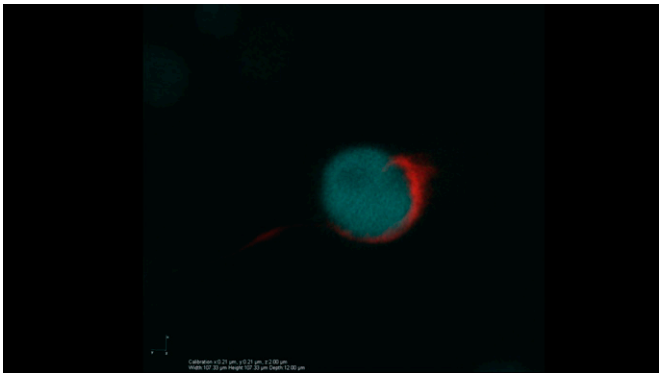

Movie S4. Asymmetric partitioning of JUNQ during division. Cells were transfected with Vimentin-mOrange2 and NLS-iRFP. No MG132 treatment.

Movie S4

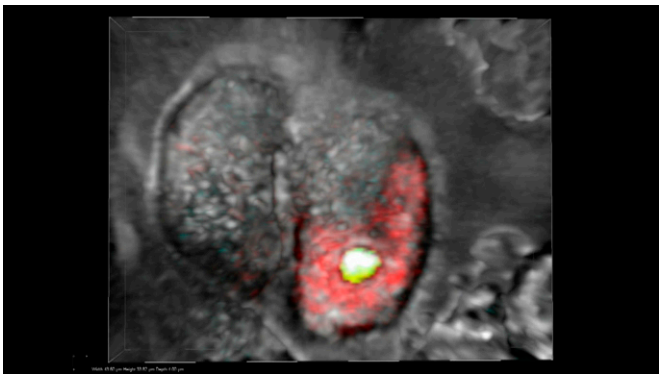

Movie S5. Asymmetric partitioning of IPOD and JUNQ to the same cell during division. Cells were transfected with HttQ119-EYFP, NLS-iRFP, and Vimentin-mOrange2. Cells were treated with 2 μM MG132 for 6 h, followed by MG132 wash-out.

Movie S5

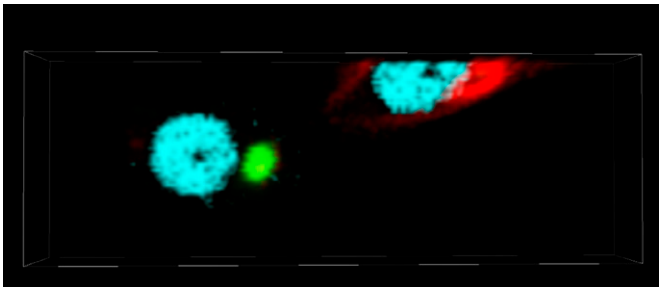

Movie S6. Partitioning of IPOD and JUNQ to different cells during division. Cells were transfected with HttQ119-EYFP, NLS-iRFP, and Vimentin-mOrange2. Cells were treated with 2 μM MG132 for 6 h, followed by MG132 wash-out.

Movie S6

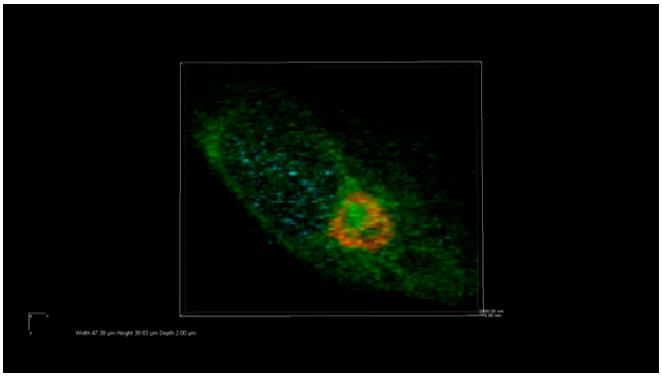

Movie S7. Vimentin JUNQ formation around the centrosome. Cells were transfected with pDendra2-α-Tubulin, NLS-iRFP, and Vimentin-mOrange2. Cells were treated with 2 μM MG132.

Movie S7

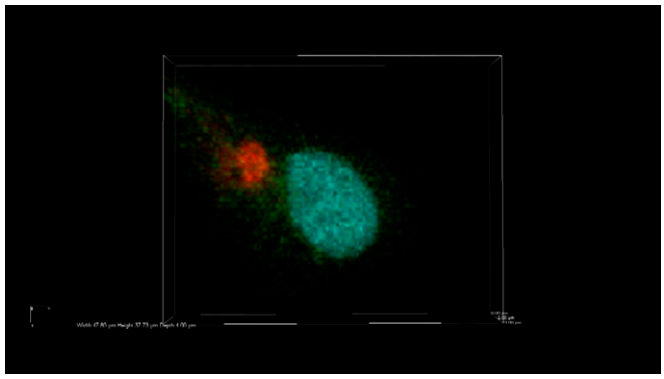

Movie S8. Vimentin JUNQ formation in cells expressing Nesprin 4. Cells were transfected with NLS-iRFP, EGFP-Nesprin 4, and Vimentin-mOrange2. Cells were treated with 2 μM MG132.

Movie S8

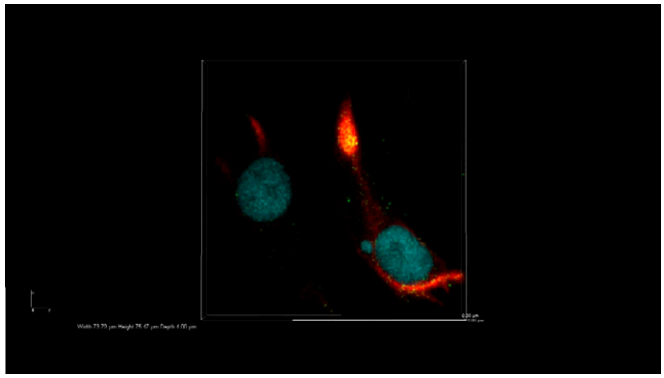

Movie S9. Vimentin JUNQ formation in cells expressing Nesprin 4. Cells were transfected with NLS-iRFP, EGFP-Nesprin 4, and Vimentin-mOrange2. Cells were treated with 5 μM MG132 for 2 h followed by MG132 wash-out.

Movie S9

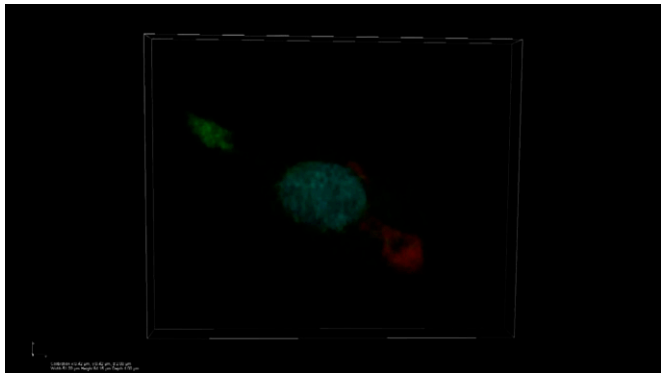

Movie S10. Vimentin JUNQ formation in cells expressing Nesprin 4 with a cell division in which the JUNQ is inherited by one cell only and is subsequently moved far from the nucleus. Cells were transfected with NLS-iRFP, pEGFP-C1-GFP-Nesprin 4, and Vimentin-mOrange2. Cells were treated with 5 μM MG132 for 2 h followed by MG132 wash-out.

Movie S10

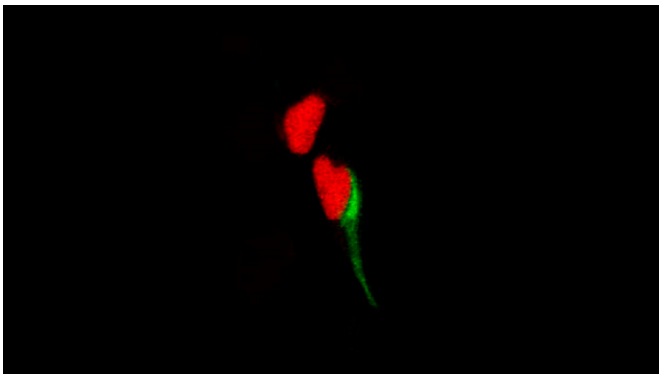

Movie S11. Vimentin JUNQ formation before mitosis and asymmetric partitioning, followed by a return to the fibrilar localization. Cells were transfected with Vimentin-tagBFP2 and NLS-iRFP.

Movie S11

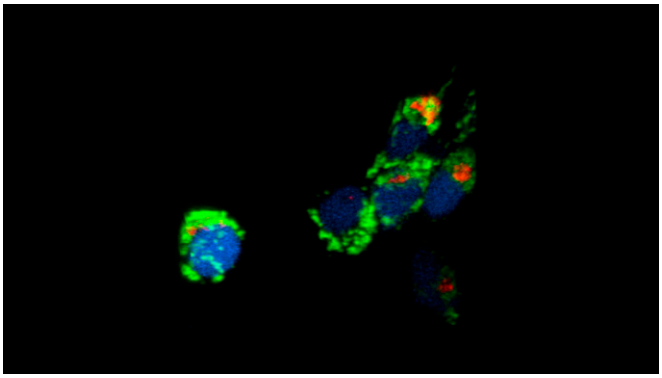

Movie S12. Two generational experiments showing that cells that fail to inherit JUNQ reach second mitosis faster than JUNQ-inheriting sister cells. Cells were transfected with Vimentin-tagBFP2, NLS-iRFP, and Mito-Dendra2.

Movie S12